Endosomal Chloride-Proton Exchange Rather Than Chloride Conductance Is Crucial for Renal Endocytosis

Gaia Novarino, *et al.*

Science **328**, 1398 (2010);
DOI: 10.1126/science.1188070

result in gB fragments that are translocated into the cytoplasm. To determine whether cytosolic access is required, we examined the roles of TAP and proteasomes in gB cross-presentation. When DCs from *Tap*$^{-/-}$ mice were incubated with necrotic infected cells, gB cross-presentation was completely eliminated (Fig. 3F). In addition, cross-presentation of gB, as well as ICP6, was inhibited by lactacystin, indicating dependence on proteasomal processing (Fig. 3E). Cross-presentation thus depends on cytosolic processing of gB fragments generated in the phagosome by GILT-mediated reduction and cathepsin-mediated proteolysis.

A requirement for GILT in the induction of the CD8$^+$ T cell response to $gB_{498\text{-}505}$ during an infection would argue that cross-priming is important for the in vivo anti–HSV-1 immune response. Wild-type and *Ifi30*$^{-/-}$ mice were infected with HSV-1, and the draining lymph nodes (LNs) were examined for the induction of K^b-$gB_{498\text{-}505}$–specific and K^b-$ICP6_{822\text{-}829}$–specific CD8$^+$ T cells. Although mice lacking GILT generated the same average percentage of $ICP6_{822\text{-}829}$-specific CD8$^+$ T cells when infected with HSV-1 as wild-type mice, the number of $gB_{498\text{-}505}$-specific CD8$^+$ T cells was significantly reduced (Fig. 4, A to C). There was no difference in the survival of the infected mice. Responses to GILT-independent epitopes such as $ICP6_{822\text{-}829}$ may make up for any deficiency.

To determine whether GILT-dependent cross-presentation is a more general phenomenon, we examined the CD8$^+$ T cell response of mice infected with the PR8 strain of influenza A virus. LN cells from naïve and infected mice were restimulated with wild-type DCs pulsed with peptides that correspond to a variety of H2-K^b– and H2-D^b–restricted epitopes from hemagglutinin (HA), neuraminidase (NA), polymerase (PA), and nucleoprotein (NP) (www.immuneepitope.com/home.do) (*22*). HA and NA contain six and eight disulfide bonds, respectively, whereas PA and NP have none (*23*–*25*). A similar percentage of wild-type and GILT-negative CD8$^+$ T cells responded to D^b-restricted PA and NP epitopes upon restimulation (Fig. 4, D and E). In contrast, the responses of CD8$^+$ T cells from mice lacking GILT were significantly reduced for four out of five of the HA epitopes and for two out of three of the NA epitopes. The two HA epitopes to which almost no CD8$^+$ T cells develop in the *Ifi30*$^{-/-}$ mice contain or are immediately adjacent to a cysteine (C480) involved in a disulfide bond (C21-C480). For both HA and NA, one epitope is GILT independent, strongly arguing against the possibility that any GILT requirement reflects GILT-dependent MHC class II–restricted responses that mediate CD4$^+$ T cell help (*26*). Although the epitope specificity of the CD4$^+$ T cells in the *Ifi30*$^{-/-}$ mice may be different from that of wild-type mice, the total numbers of CD4$^+$ T cells that they generate during a viral immune response are similar (fig. S2), as are the numbers of CD4$^+$ T cells in the spleens of uninfected wild-type and *Ifi30*$^{-/-}$ mice. The data show that GILT-dependent cross-presentation is not restricted to gB, and that cross-priming is important in the CD8$^+$ T cell response to influenza virus. The residual CD8$^+$ T cell responses observed to gB and the HA and NA epitopes by *Ifi30*$^{-/-}$ animals may reflect priming by directly infected APCs.

The only known function of GILT is to reduce disulfide bonds, and we have shown that GILT is essential for cross-presentation of many peptides from disulfide-containing proteins. We suggest that reduction in the acidic environment of the phagosome facilitates partial proteolysis into fragments that are translocated into the cytosol where they are further degraded by the proteasome to generate peptides. These are transported by TAP and bind in a conventional manner, possibly after amino-terminal trimming (*27*), to MHC class I molecules. This latter step is likely to occur in the ER, but could occur in phagosomes that have recruited ER membrane components, although this issue remains contentious (*28*, *29*).

For gB, the inability to cross-present is reflected in a reduction in K^b-$gB_{498\text{-}505}$–specific CD8$^+$ T cells in vivo, indicating the importance of cross-priming in CD8$^+$ T cell responses to HSV-1 infection. The similar reduction in HA- and NA-specific CD8$^+$ T cells suggests that cross-priming is also important during influenza A infection. The role played by GILT in cross-priming, combined with its established involvement in MHC class II–restricted CD4$^+$ T cell responses (*30*), indicates the importance of the enzyme in the immune system. This may have implications for vaccine design and approaches to tumor immunotherapy that involve peptide-based vaccines, in that linear peptides may not be the optimal vehicles for the expression of GILT-dependent epitopes, and for autoimmunity to self-antigens that contain multiple disulfide bonds.

References and Notes

1. M. J. Bevan, *J. Exp. Med.* **143**, 1283 (1976).
2. L. J. Sigal, S. Crotty, R. Andino, K. L. Rock, *Nature* **398**, 77 (1999).
3. K. L. Rock, L. Shen, *Immunol. Rev.* **207**, 166 (2005).
4. R. S. Allan *et al.*, *Immunity* **25**, 153 (2006).
5. S. Bedoui *et al.*, *Nat. Immunol.* **10**, 488 (2009).
6. R. Belizaire, E. R. Unanue, *Proc. Natl. Acad. Sci. U.S.A.* **106**, 17463 (2009).
7. M. Kovacsovics-Bankowski, K. L. Rock, *Science* **267**, 243 (1995).
8. A. L. Ackerman, A. Giodini, P. Cresswell, *Immunity* **25**, 607 (2006).
9. A. Schäfer, D. H. Wolf, *EMBO J.* **28**, 2874 (2009).
10. M. L. Lin *et al.*, *Proc. Natl. Acad. Sci. U.S.A.* **105**, 3029 (2008).
11. C. C. Norbury, B. J. Chambers, A. R. Prescott, H. G. Ljunggren, C. Watts, *Eur. J. Immunol.* **27**, 280 (1997).
12. A. Giodini, P. Cresswell, *EMBO J.* **27**, 201 (2008).
13. B. Arunachalam, U. T. Phan, H. J. Geuze, P. Cresswell, *Proc. Natl. Acad. Sci. U.S.A.* **97**, 745 (2000).
14. U. T. Phan, B. Arunachalam, P. Cresswell, *J. Biol. Chem.* **275**, 25907 (2000).
15. T. Hanke, F. L. Graham, K. L. Rosenthal, D. C. Johnson, *J. Virol.* **65**, 1177 (1991).
16. See supporting material on *Science* Online.
17. E. E. Heldwein *et al.*, *Science* **313**, 217 (2006).
18. R. Singh, A. Jamieson, P. Cresswell, *Nature* **455**, 1244 (2008).
19. D. S. Collins, E. R. Unanue, C. V. Harding, *J. Immunol.* **147**, 4054 (1991).
20. K. L. McCoy *et al.*, *J. Immunol.* **143**, 29 (1989).
21. A. Savina *et al.*, *Cell* **126**, 205 (2006).
22. W. Zhong, P. A. Reche, C. C. Lai, B. Reinhold, E. L. Reinherz, *J. Biol. Chem.* **278**, 45135 (2003).
23. J. N. Varghese, W. G. Laver, P. M. Colman, *Nature* **303**, 35 (1983).
24. I. A. Wilson, J. J. Skehel, D. C. Wiley, *Nature* **289**, 366 (1981).
25. Q. Ye, R. M. Krug, Y. J. Tao, *Nature* **444**, 1078 (2006).
26. N. K. Rajasagi *et al.*, *J. Virol.* **83**, 5256 (2009).
27. T. Serwold, F. Gonzalez, J. Kim, R. Jacob, N. Shastri, *Nature* **419**, 480 (2002).
28. I. Jutras, M. Desjardins, *Annu. Rev. Cell Dev. Biol.* **21**, 511 (2005).
29. N. Touret *et al.*, *Cell* **123**, 157 (2005).
30. M. Maric *et al.*, *Science* **294**, 1361 (2001).

31. This work was supported by the Howard Hughes Medical Institute and NIH grant R37AI23081 (P.C.).

Supporting Online Material

www.sciencemag.org/cgi/content/full/328/5984/1394/DC1
Materials and Methods
Figs. S1 and S2
References

5 March 2010; accepted 4 May 2010
10.1126/science.1189176

Endosomal Chloride-Proton Exchange Rather Than Chloride Conductance Is Crucial for Renal Endocytosis

Gaia Novarino, Stefanie Weinert, Gesa Rickheit,* Thomas J. Jentsch†

Loss of the endosomal anion transport protein ClC-5 impairs renal endocytosis and underlies human Dent's disease. ClC-5 is thought to promote endocytosis by facilitating endosomal acidification through the neutralization of proton pump currents. However, ClC-5 is a 2 chloride (Cl^-)/proton (H^+) exchanger rather than a Cl^- channel. We generated mice that carry the uncoupling E211A (unc) mutation that converts ClC-5 into a pure Cl^- conductor. Adenosine triphosphate (ATP)–dependent acidification of renal endosomes was reduced in mice in which ClC-5 was knocked out, but normal in *Clcn5*^{unc} mice. However, their proximal tubular endocytosis was also impaired. Thus, endosomal chloride concentration, which is raised by ClC-5 in exchange for protons accumulated by the H^+-ATPase, may play a role in endocytosis.

Luminal acidification along the endocytic pathway serves many purposes (*1*), including the progression of endocytosis itself (*2*). It is performed by endosomal H^+-transporting adenosine triphosphatases (H^+-ATPases) that need a countercurrent for electroneutrality. Because this

current depends on chloride, conventional wisdom suggests (*1*) that endosomal Cl^- channels are involved (fig. S1A). ClC-5 was thought to embody this channel in proximal tubular endosomes (*3*–*5*). Disruption of ClC-5 impairs renal endosomal acidification in vitro (*5*) and drastically reduces proximal tubular endocytosis in mice and humans (*4*, *6*, *7*). The hyperphosphaturia and hypercalciuria that lead to kidney stones in Dent's disease have been attributed to impaired tubular endocytosis of calciotropic hormones (*4*). However, it has recently been shown (*8*–*10*) that ClC-5 is a $2Cl^-/H^+$ exchanger rather than a Cl^- channel. It seems counterintuitive that such an exchanger should neutralize pump currents because it mediates H^+-efflux during ATP-driven acidification. The biological consequence of proton coupling has remained enigmatic (*11*).

If the ClC-5 Cl^-/H^+ exchanger could be converted into an uncoupled Cl^- conductor, it should efficiently facilitate endosomal acidification. Phenotypes of mice carrying such a mutation cannot be attributed to impaired endosomal acidification, but can be ascribed specifically to a loss of coupling chloride gradients to proton gradients. A mutation in the "gating" glutamate of CLC exchangers (*12*) suffices to convert them into pure anion conductors (*8*, *9*, *13*–*15*). We inserted the corresponding, well-characterized E211A mutation (*8*, *9*, *14*, *16*, *17*) into the *Clcn5* gene on mouse chromosome X and created mice in which ClC-5 was converted into an uncoupled Cl^- conductor (*Clcn5*^{unc} mice) (figs. S1A and S2). The mutant protein was expressed at wild-type (WT) levels (Fig. 1A). No change was observed in its subcellular localization in kidney proximal tubular and intercalated cells (Fig. 1B and fig. S3). The renal expression of the related ClC-3 and ClC-4 proteins also was not affected (fig. S4).

To test whether the uncoupled ClC-5^{unc} mutant supported endosomal acidification, we added ATP to endosomal fractions from renal cortex (containing mainly proximal tubules) of WT or *Clcn5*$^{unc/y}$ mice and monitored vesicular pH using acridine orange fluorescence. H^+-ATPase–driven acidification of WT and *Clcn5*^{unc} vesicles occurred with similar efficiency but was severely reduced with endosomes from mice in which ClC-5 was knocked out (KO mice), as expected (*5*, *18*) (Fig. 1, C to E).

Despite maintaining active endosomal acidification, *Clcn5*^{unc} mice displayed abnormalities found in ClC-5 KO (*Clcn5*$^-$) mice and patients with Dent's disease (*4*, *7*, *19*), such as low-molecular-weight proteinuria (Fig. 2, A and B), hyperphosphaturia, and hypercalciuria (table S1). Proteinuria of *Clcn5*$^-$ mice results from impaired proximal tubular endocytosis (*4*, *7*), which was studied in chimeric tubules resulting from random X-chromosomal inactivation in female *Clcn5*$^{+/-}$ mice (*4*). In those tubules, WT and KO cells were distinguished by means of antibodies to ClC-5 (*3*, *4*), but this approach cannot differentiate between cells expressing the WT or uncoupled ClC-5 in *Clcn5*$^{unc/+}$ tubules. Rather than epitope-tagging the E211A mutant, which might interfere with its function, we generated mice in which the C terminus of ClC-5 was converted to that of ClC-3 (fig. S1, B and C, and S5). The generation of this *Clcn5** allele required only two amino acid exchanges and changed neither ClC-5 currents (fig. S5D) nor its abundance (Fig. 1A) and localization (fig. S6A). Our antibodies against the C terminus of ClC-5 recognized ClC-5 and ClC-5^{unc} but not ClC-5* (Figs. 1A and 2, C and D, and fig. S1, B and C). In vivo endocytosis experiments were performed by injecting into the bloodstream labeled endocytic cargo that can pass the glomerular filter. Endocytosis in cells expressing the *Clcn5** allele or WT ClC-5 was indistinguishable (fig. S6B). However, cells expressing the *Clcn5*^{unc} allele accumulated much less fluorescently labeled β-lactoglobulin, which is a marker for receptor-mediated endocytosis (Fig. 2C), or the fluid-phase marker dextran (Fig. 2D) than did neighboring cells that express the $2Cl^-/H^+$–exchanger ClC-5*. Thus, uncoupling anion transport from protons resulted in a cell-autonomous impairment of both receptor-mediated and fluid-phase endocytosis akin to *Clcn5*$^-$ mice (*4*). Similarly as in KO mice (*4*, *20*), cells expressing the uncoupled E211A mutant displayed reduced levels of the endocytic receptors megalin (Fig. 3, A and C) and cubilin (Fig. 3B)—a finding ascribed to impaired recycling to the plasma membrane (*4*, *20*). In *Clcn5*^{unc} kidney, the sodium-phosphate cotransporter NaPi-2a was shifted from the apical membrane to intracellular vesicles, and its overall abundance was reduced (fig. S7), which explains the observed hyperphosphaturia. Similarly increased endocytosis of NaPi-2a in *Clcn5*$^-$ mice was attributed to reduced endocytosis of filtered parathyroid hormone (PTH), entailing a luminal increase of PTH and excessive stimulation of apical PTH receptors (*4*, *5*).

Because the E211A mutation did not abolish ClC-5 currents and maintained endosomal acidification (Fig. 1C), it might have affected endocytosis less than a loss of ClC-5. We thus compared *Clcn5*^{unc} and *Clcn5*$^-$ cells side by side in chimeric tubules of *Clcn5*$^{unc/-}$ females. No differences were detected in receptor-mediated (Fig. 2E) or fluid-phase endocytosis (fig. S8), nor in the localization and abundance of megalin (Fig. 3C). Thus unexpectedly, the anion conductance of ClC-5(E211A) could not even partially substitute for Cl^-/H^+ exchange in the support of proximal tubular endocytosis and normal localization of apical receptors.

Because the intramembrane E211A point mutation was unlikely to have changed ClC-5 protein interactions, the pathology of *Clcn5*^{unc} mice is caused neither by the disruption of a macromolecular ClC-5–containing endocytic complex (*21*, *22*) nor by the loss of interaction with KIF3B

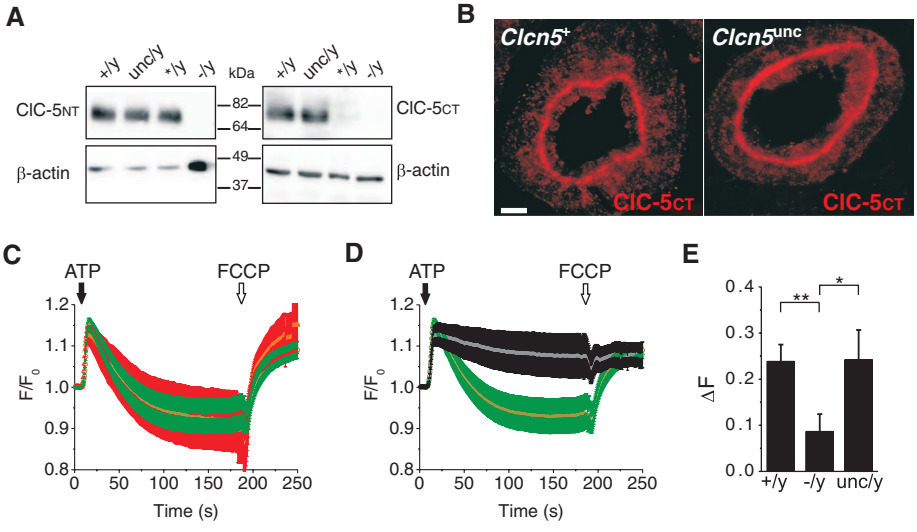

Fig. 1. Renal endosomal acidification of mice converting ClC-5 into a chloride conductor. (**A**) Immunoblot for ClC-5 using kidney membranes of different genotypes with antibodies against the (left) N terminus or the (right) C terminus (C5/05A). Asterisk indicates mutated C terminus of ClC-5 (fig. S5). (**B**) Identical staining pattern using the C-terminal PEP5E antibody to ClC-5 (*3*) in proximal tubules of WT and *Clcn5*$^{unc/y}$ mice. Scale bar, 5 μm. (**C** and **D**) Averaged traces of acridine orange fluorescence comparing ATP-driven acidification of renal cortical vesicles from (C) WT (green) and *Clcn5*^{unc} (red) and (D) WT (green) and *Clcn5*$^-$ (black) mice (with identical WT traces). Reduced fluorescence reflects vesicular acidification. The protonophore FCCP was added as a control. F_0, fluorescence at time (t) = 0. (**E**) Averaged total change in fluorescence. Data averaged from 25 (+/y), 13 (–/y), and 10 (unc/y) experiments with material obtained from more than four independent vesicle preparations per genotype. Error bars, SEM. *$P \leq 0.05$; **$P \leq 0.01$.

Leibniz-Institut für Molekulare Pharmakologie (FMP) and Max-Delbrück-Centrum für Molekulare Medizin (MDC), 13125 Berlin, Germany.

*Present address: TaconicArtemis GmbH, 51063 Köln, Germany.

†To whom correspondence should be addressed. E-mail: jentsch@fmp-berlin.de

(*23*), which are mechanisms that have been suggested to underlie Dent's disease. The impairment of endocytosis in Dent's disease is not likely to result only from reduced ATP-dependent endosomal acidification (*3*) but is related to an uncoupling of Cl^- gradients from H^+ gradients. ClC-5 might drive H^+-ATPase–independent acidification by exchanging cytosolic H^+ for intravesicular Cl^- at an early step of endocytosis (*9*). Shortly after pinching off from the plasma membrane, endocytic vesicles may contain the high extracellular chloride concentration. A selective lack of such an initial Cl^- gradient–driven endosomal acidification might explain the impaired endocytosis of both *Clcn5*$^-$ and *Clcn5*^{unc} mice. However, endosomal [Cl^-] was found to be initially low—a finding ascribed to surface charge effects (*18*). Furthermore, a lack of a Cl^- gradient–driven acidification cannot be invoked for the severe lysosomal pathology of *Clcn7*$^{-/-}$ (*24*, *25*) and *Clcn7*$^{unc/unc}$ mice (*26*) because their lysosomal pH is normal (*24*–*26*) and because this mechanism would require a substantial Cl^- supply to lysosomes.

The surprisingly similar pathologies of *Clcn5*$^-$ and *Clcn5*^{unc} mice might be due to reduced endosomal Cl^- accumulation in each mouse model. Whereas Cl^- channels operating in parallel to an H^+-ATPase would raise intravesicular Cl^- during active acidification, stoichiometric $2Cl^-/H^+$ exchange would maintain high vesicular Cl^- concentration also under steady state. Indeed, lysosomes containing the WT ClC-7 Cl^-/H^+ exchanger display higher [Cl^-] than their *Clcn7*$^{-/-}$ or *Clcn7*$^{unc/unc}$ counterparts (*26*). Furthermore, endosomal [Cl^-] might regulate endosomal Ca^{++} channels (*27*). The analysis of *Clcn5*^{unc} and *Clcn7*^{unc} (*26*) mice suggests that luminal anion concentration is important all along the endosomal-lysosomal pathway.

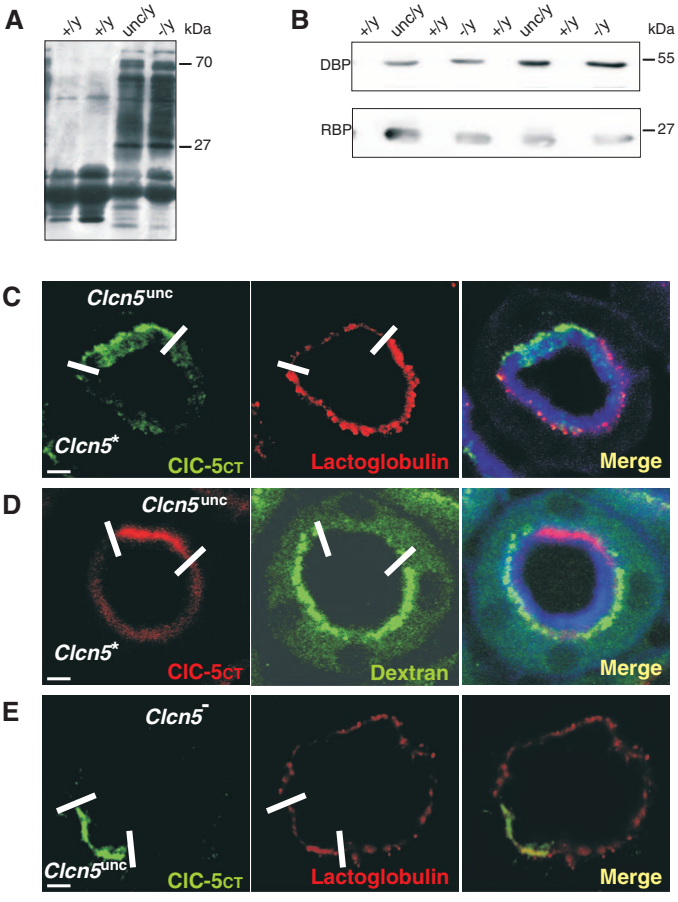

Fig. 2. Proteinuria and impaired endocytosis in *Clcn5*$^-$ *Clcn5*^{unc} mice. (**A**) Urinary proteins analyzed by means of SDS–polyacrylamide gel electrophoresis and silver staining. (**B**) Immunoblot for vitamin D–binding protein (DBP) and retinol-binding protein (RBP) in urine. (**C**) In vivo 10-min uptake of Alexa Fluor 546–labeled (Invitrogen, Carlsbad, CA) β-lactoglobulin (red) showed decreased receptor-mediated endocytosis in *Clcn5*^{unc}-expressing cells in a chimeric proximal tubule from a *Clcn5*$^{unc/*}$ female. ClC-5^{unc}, but not the ClC-5* Cl^-/H^+ exchanger, is recognized by the antibody C5/05A (green). (Right) Overlay with additional brush-border staining for villin (blue). (**D**) Reduced fluid-phase endocytosis of Alexa Fluor 488–labeled (Invitrogen) dextran in ClC-5^{unc}–expressing cells in an experiment similar to (C). (**E**) Similar β-lactoglobulin–uptake of cells lacking ClC-5 or expressing *Clcn5*^{unc} in a *Clcn5*$^{unc/-}$ female. Scale bars, 5 μm (C), 3.2 μm (D), and 6 μm (E).

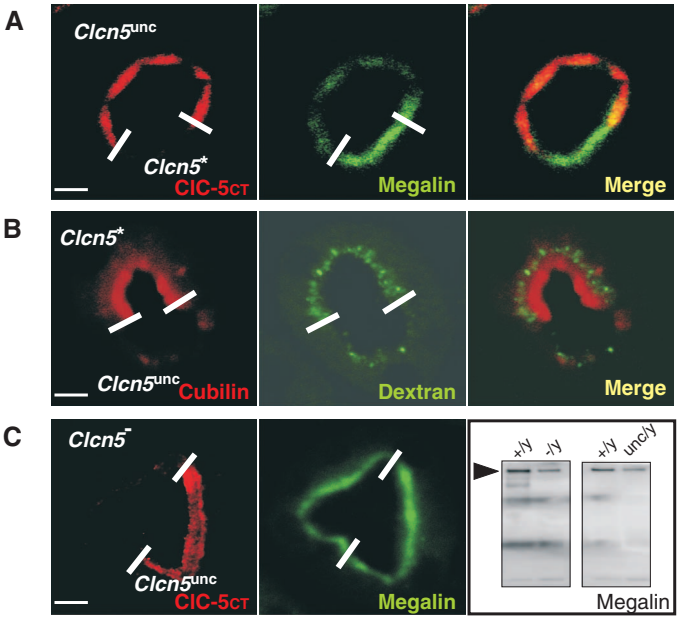

Fig. 3. Effect of uncoupling ClC-5 on endocytic receptors. (**A**) Reduced megalin levels in *Clcn5*^{unc}-expressing cells of a chimeric tubule of *Clcn5*$^{unc/*}$ mice. (**B**) Reduced cubilin expression in *Clcn5*^{unc}-expressing cells that were identified through reduced endocytosis of Alexa 488–dextran. (**C**) Similar reduction of megalin in cells expressing *Clcn5*$^-$ or *Clcn5*^{unc}. To compare weak megalin immunostaining in *Clcn5*$^{unc/-}$ tubules, image intensity was boosted in the center panel as compared with that of (A). (Right) Immunoblot for megalin using kidney membranes from WT, *Clcn5*$^{unc/y}$, and *Clcn5*$^{-/y}$ mice. Scale bars, 4 μm [(A) and (B)] and 5 μm (C).

References and Notes

1. I. Mellman, R. Fuchs, A. Helenius, *Annu. Rev. Biochem.* **55**, 663 (1986).
2. M. J. Clague, S. Urbé, F. Aniento, J. Gruenberg, *J. Biol. Chem.* **269**, 21 (1994).
3. W. Günther, A. Lüchow, F. Cluzeaud, A. Vandewalle, T. J. Jentsch, *Proc. Natl. Acad. Sci. U.S.A.* **95**, 8075 (1998).
4. N. Piwon, W. Günther, M. Schwake, M. R. Bösl, T. J. Jentsch, *Nature* **408**, 369 (2000).
5. W. Günther, N. Piwon, T. J. Jentsch, *Pflügers Arch.* **445**, 456 (2003).
6. S. E. Lloyd *et al.*, *Nature* **379**, 445 (1996).
7. S. S. Wang *et al.*, *Hum. Mol. Genet.* **9**, 2937 (2000).
8. A. Picollo, M. Pusch, *Nature* **436**, 420 (2005).
9. O. Scheel, A. A. Zdebik, S. Lourdel, T. J. Jentsch, *Nature* **436**, 424 (2005).
10. G. Zifarelli, M. Pusch, *EMBO J.* **28**, 175 (2009).
11. T. J. Jentsch, *J. Physiol.* **578**, 633 (2007).
12. R. Dutzler, E. B. Campbell, R. MacKinnon, *Science* **300**, 108 (2003).
13. A. Accardi, C. Miller, *Nature* **427**, 803 (2004).
14. A. A. Zdebik *et al.*, *J. Biol. Chem.* **283**, 4219 (2007).
15. E. Y. Bergsdorf, A. A. Zdebik, T. J. Jentsch, *J. Biol. Chem.* **284**, 11184 (2009).
16. In the mutants, other amino acids were substituted at certain locations; for example, E211A indicates that glutamic acid at position 211 was replaced by alanine. Single-letter abbreviations for the amino acid residues are as follows: A, Ala; C, Cys; D, Asp; E, Glu; F, Phe; G, Gly; H, His; I, Ile; K, Lys; L, Leu; M, Met; N, Asn; P, Pro; Q, Gln; R, Arg; S, Ser; T, Thr; V, Val; W, Trp; and Y, Tyr.
17. Materials and methods are available as supporting material on *Science* Online.
18. M. Hara-Chikuma, Y. Wang, S. E. Guggino, W. B. Guggino, A. S. Verkman, *Biochem. Biophys. Res. Commun.* **329**, 941 (2005).
19. S. J. Scheinman, *Kidney Int.* **53**, 3 (1998).
20. E. I. Christensen *et al.*, *Proc. Natl. Acad. Sci. U.S.A.* **100**, 8472 (2003).
21. D. H. Hryciw *et al.*, *J. Biol. Chem.* **278**, 40169 (2003).
22. D. H. Hryciw *et al.*, *J. Biol. Chem.* **281**, 16068 (2006).
23. A. A. Reed *et al.*, *Am. J. Physiol. Renal Physiol.* **298**, F365 (2010).

24. D. Kasper *et al.*, *EMBO J.* **24**, 1079 (2005).
25. P. F. Lange, L. Wartosch, T. J. Jentsch, J. C. Fuhrmann, *Nature* **440**, 220 (2006).
26. S. Weinert *et al.*, *Science* **328**, 1401 (2010); published online 29 April 2010 (10.1126/science.1188072).
27. M. Saito, P. I. Hanson, P. Schlesinger, *J. Biol. Chem.* **282**, 27327 (2007).
28. We thank R. Pareja-Alcaraz and S. Rode for technical assistance and P. Verroust, S. Bachmann, W. Blaner, and C. Wagner for antibodies against cubilin, megalin, retinol binding protein, and AE1, respectively. This work was supported by the Deutsche Forschungsgemeinschaft (grants Zd58/1, Je164/6, and Je164/9).

Supporting Online Material
www.sciencemag.org/cgi/content/full/science.1188070/DC1
Materials and Methods
Figs. S1 to S8
Table S1
References

8 February 2010; accepted 21 April 2010
Published online 29 April 2010;
10.1126/science.1188070
Include this information when citing this paper.

Lysosomal Pathology and Osteopetrosis upon Loss of H^+-Driven Lysosomal Cl^- Accumulation

Stefanie Weinert,[1,2] Sabrina Jabs,[1,2,6] Chayarop Supanchart,[3] Michaela Schweizer,[4] Niclas Gimber,[1,2] Martin Richter,[1,6] Jörg Rademann,[1,6]* Tobias Stauber,[1,2] Uwe Kornak,[3,5] Thomas J. Jentsch[1,2]†

During lysosomal acidification, proton-pump currents are thought to be shunted by a chloride ion (Cl^-) channel, tentatively identified as ClC-7. Surprisingly, recent data suggest that ClC-7 instead mediates Cl^-/proton (H^+) exchange. We generated mice carrying a point mutation converting ClC-7 into an uncoupled (unc) Cl^- conductor. Despite maintaining lysosomal conductance and normal lysosomal pH, these *Clcn7*$^{unc/unc}$ mice showed lysosomal storage disease like mice lacking ClC-7. However, their osteopetrosis was milder, and they lacked a coat color phenotype. Thus, only some roles of ClC-7 Cl^-/H^+ exchange can be taken over by a Cl^- conductance. This conductance was even deleterious in *Clcn7*$^{+/unc}$ mice. *Clcn7*$^{-/-}$ and *Clcn7*$^{unc/unc}$ mice accumulated less Cl^- in lysosomes than did wild-type mice. Thus, lowered lysosomal chloride may underlie their common phenotypes.

ClC-7 is the only member of the CLC gene family of anion transporters substantially expressed on lysosomes (*1*–*3*), where it resides together with its β-subunit Ostm1 (*3*). Inactivation of either subunit leads to lysosomal storage disease and osteopetrosis in mice and humans (*1*–*4*). Cellular defects include slowed degradation of endocytosed proteins (*5*) and impaired acidification of the osteoclast resorption lacuna (*1*). Cl^- currents mediated by ClC-7 have been deemed necessary for shunting lysosomal proton-pump currents (*1*). However, lysosomal pH was normal in cells lacking either ClC-7 or Ostm1 (*2*, *3*). ClC-7 now seems likely to be a Cl^-/H^+ exchanger rather than a Cl^- channel (*6*, *7*). Because H^+-pump currents may be neutralized by both Cl^- channels and electrogenic Cl^-/H^+ exchangers (*6*), it is unclear whether lysosomal Cl^-/H^+ exchange confers functional advantages over the simple Cl^- conductance in the textbook model for vesicular acidification.

We created knock-in mice in which the ClC-7 "gating" glutamate (E) was mutated to alanine (A) (fig. S1) (*8*). On the basis of results from other CLC Cl^-/H^+ exchangers (*9*–*12*), this $Glu^{245} \rightarrow Ala^{245}$ (E245A) mutation should lead to Cl^- transport that is uncoupled (unc) from protons, hence our designation of this allele as *Clcn7*^{unc}. Homozygous *Clcn7*$^{unc/unc}$ mice showed severe growth retardation (Fig. 1A and fig. S2) and died within 5 weeks. ClC-7^{unc} and wild-type (WT) ClC-7 were expressed at similar levels (Fig. 1B) and similarly localized to lysosomes (Fig. 1D). Neither the abundance, nor the lysosomal localization of Ostm1 was changed in *Clcn7*$^{unc/unc}$ mice, contrasting with its strongly reduced protein level (*3*) and mislocalization in *Clcn7*$^{-/-}$ cells (Fig. 1, C and D). In neurons, however, ClC-7^{unc} staining was more diffuse (fig. S3B), reflecting changed lysosomal compartments like in *Clcn7*$^{-/-}$ neurons (*2*). The abundance of other CLC exchangers was unchanged in *Clcn7*$^{unc/unc}$ mice (fig. S4).

In an *agouti* genetic background, the coat color of *Clcn7*$^{-/-}$ and *Ostm1*$^{-/-}$ (*grey-lethal*) mice is grey (*3*, *4*), whereas it was brownish in WT and *Clcn7*$^{unc/unc}$ mice (Fig. 1A). *Clcn7*$^{unc/unc}$ mice were osteopetrotic (Fig. 2A and fig. S5), although less severely than *Clcn7*$^{-/-}$ (*1*) or *Ostm1*$^{-/-}$ (*4*) mice. ClC-7 and Ostm1 were detected at the ruffled border of *Clcn7*$^{unc/unc}$ osteoclasts (fig. S3A). This

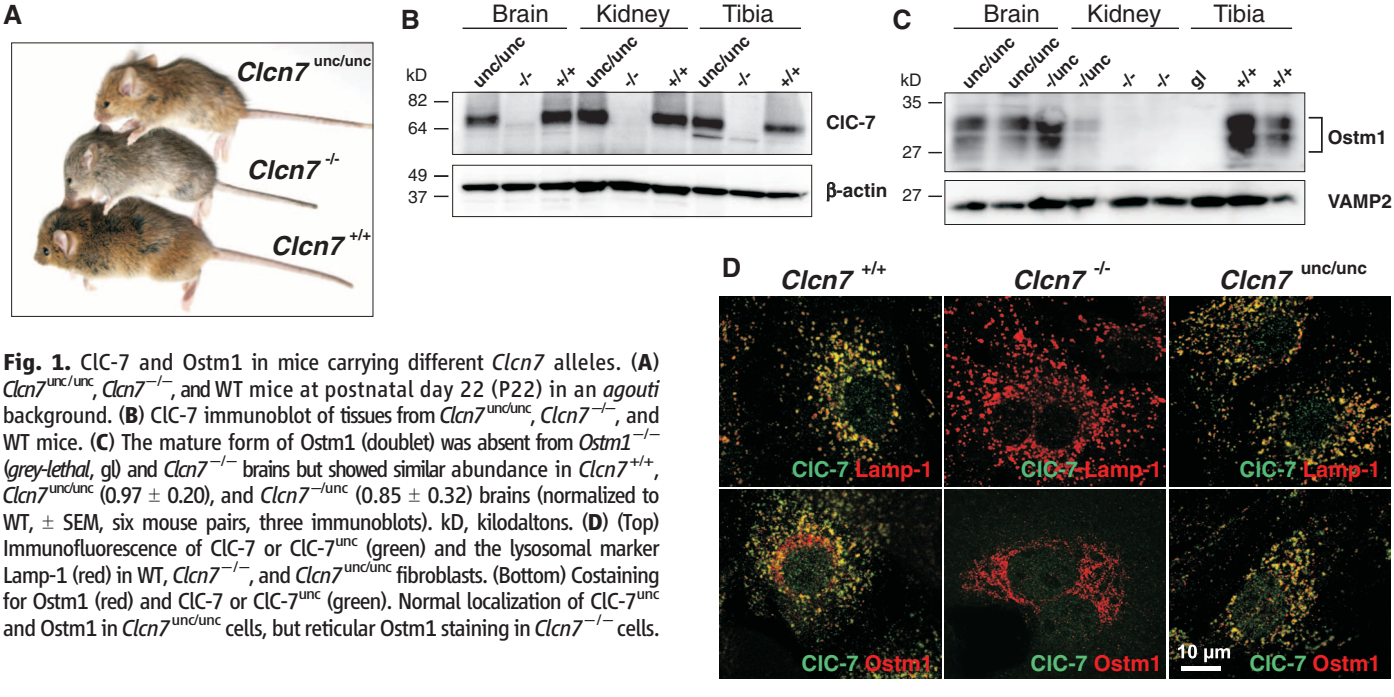

Fig. 1. ClC-7 and Ostm1 in mice carrying different *Clcn7* alleles. (**A**) *Clcn7*$^{unc/unc}$, *Clcn7*$^{-/-}$, and WT mice at postnatal day 22 (P22) in an *agouti* background. (**B**) ClC-7 immunoblot of tissues from *Clcn7*$^{unc/unc}$, *Clcn7*$^{-/-}$, and WT mice. (**C**) The mature form of Ostm1 (doublet) was absent from *Ostm1*$^{-/-}$ (*grey-lethal*, gl) and *Clcn7*$^{-/-}$ brains but showed similar abundance in *Clcn7*$^{+/+}$, *Clcn7*$^{unc/unc}$ (0.97 ± 0.20), and *Clcn7*$^{-/unc}$ (0.85 ± 0.32) brains (normalized to WT, ± SEM, six mouse pairs, three immunoblots). kD, kilodaltons. (**D**) (Top) Immunofluorescence of ClC-7 or ClC-7^{unc} (green) and the lysosomal marker Lamp-1 (red) in WT, *Clcn7*$^{-/-}$, and *Clcn7*$^{unc/unc}$ fibroblasts. (Bottom) Costaining for Ostm1 (red) and ClC-7 or ClC-7^{unc} (green). Normal localization of ClC-7^{unc} and Ostm1 in *Clcn7*$^{unc/unc}$ cells, but reticular Ostm1 staining in *Clcn7*$^{-/-}$ cells.